

pubs.acs.org/JPCA Article

Comprehensive Analysis of Products and the Development of a Quantitative Mechanism for the OH Radical-Initiated Oxidation of 1-Alkenes in the Presence of NO_x

Julia G. Bakker-Arkema and Paul J. Ziemann*



Cite This: J. Phys. Chem. A 2021, 125, 5829-5840



ACCESS I

III Metrics & More

Article Recommendations

s Supporting Information

ABSTRACT: The reactions of 1-tetradecene and 1-pentadecene, the C_{14} and C_{15} linear 1-alkenes, with OH radicals in the presence of NO_x were investigated in a series of environmental chamber experiments. Particle-phase β-hydroxynitrates, dihydroxynitrates, dihydroxycarbonyls, and 1,4-hydroxynitrates and gas-phase aldehydes were sampled and then identified and quantified using a suite of offline analytical techniques that included derivatization, gas and liquid chromatography, and multiple types of mass spectrometry. Measured molar yields of products formed by OH radical addition to the C=C double bond, including β-hydroxynitrates, dihydrox-

ynitrates, dihydroxycarbonyls (which have not been previously directly quantified with high accuracy), and aldehydes were 0.125 \pm 0.01, 0.048 \pm 0.005, 0.240 \pm 0.04, and 0.268 \pm 0.03 (0.264 \pm 0.02 and 0.271 \pm 0.04 for the formaldehyde and tridecanal/tetradecanal co-products of β-hydroxyalkoxy radical decomposition), respectively. These values give a total molar yield of 0.681 \pm 0.05, which agrees very well with the results of kinetics measurements that indicate that the fraction of reaction that occurs by OH radical addition is 0.70. The yields were used to calculate branching ratios for all OH radical addition pathways, including a value of 0.18 for the formation of dihydroxynitrates from the reaction of dihydroxyperoxy radicals with NO and values of 0.47 and 0.53 for β-hydroxyalkoxy radical decomposition and isomerization. The results were used with literature data on the yields of aldehydes measured for similar reactions of smaller alkenes, a model for the effect of carbon number on branching ratios for organic nitrate formation, and a mechanism for H atom abstraction derived from studies of linear alkanes to achieve a complete, quantitative gasphase reaction mechanism for 1-alkenes. The results should also be useful for constructing mechanisms for more complex reactions of volatile organic compounds.

■ INTRODUCTION

Of the estimated ~1150 Tg of nonmethane volatile organic compounds (VOCs) emitted each year to the atmosphere, more than half are alkenes, which react primarily with OH radicals, NO₃ radicals, and O₃ to form more oxygenated products. When the reaction products have sufficiently low vapor pressures, they can condense to form secondary organic aerosol (SOA), which can impact visibility, climate, and human health.² Due to the importance of alkenes to atmospheric chemistry and SOA formation, several previous studies have attempted to determine product yields and elucidate oxidation mechanisms for reactions of isoprene and monoterpenes,^{3,4} which make up ~50 and ~15% of total biogenic VOC emissions, respectively.⁵ This information is crucial for explicit modeling of atmospheric VOC oxidation and SOA formation.⁶ However, because of the large number and complex structures of products formed from these reactions, comprehensive molecular analysis is challenging. Furthermore, products of these reactions can often exist in both the gas and particle phases, and also partition to the walls of chambers used in experiments.

Although simple linear and branched monoalkenes are emitted to the atmosphere in much smaller amounts than terpenes,⁷ there are benefits to studying these simpler systems. The carbon chain length can be easily varied to shift the vapor pressures of reaction products and thus preferentially form compounds that exist predominantly in either the gas or particle phase, and the simpler structures lead to fewer reaction products. Comprehensive understanding of the oxidation products and mechanisms of simpler alkenes can then serve as useful models, providing insights into more complex reactions, and also in some cases allowing measurements of branching ratios for fundamental reaction pathways that can be applied to other systems. Although a few product studies have been conducted on reactions of simple alkenes, ⁸⁻¹³ none have been comprehensive, primarily because of the analytical

 Received:
 April 24, 2021

 Revised:
 June 12, 2021

 Published:
 June 25, 2021





challenges. For example, the major products of the reactions of linear alkenes with OH radicals in the presence of NO_x contain nitrate, hydroxyl, and carbonyl functional groups; ¹⁴ and products formed from different pathways (functionalization vs fragmentation) have a large range of volatilities, thus requiring multiple techniques for collection and analysis. Furthermore, even for simple alkenes, most reaction products are not commercially available for use as standards, making product identification and quantification difficult.

In this study, we identified and quantified the major gas- and particle-phase products formed from the reactions of the C_{14} and C_{15} 1-alkenes with OH radicals in the presence of NO_x . These included dihydroxycarbonyls, which have not been previously quantified with high accuracy. The molar yields of the products were used to quantify branching ratios for reaction pathways, and then summed to determine the extent to which mass balance was achieved. The results demonstrate the potential for comprehensively and accurately analyzing the complex chemical composition of products formed in the oxidation of organic compounds in environmental chamber studies.

■ EXPERIMENTAL SECTION

Chemicals. The following chemicals were used in this study: 1-tetradecene (96%), 1-pentadecene (98%), tridecanal $(\geq 95\%)$, tetradecanal (97%), 2-ethylhexyl nitrate (97%), O-(2,3,4,5,6-pentafluorobenzyl)hydroxylamine hydrochloride (≥99%), dioctyl phthalate (99%), and acetonitrile (highperformance liquid chromatography (HPLC) grade) from Sigma-Aldrich; 2,4-dinitrophenylhydrazine (97%) from Aldrich; 6-hydroxy-5-decanone (≥97%) from TCI; formaldehyde (37% in water, ACS Reagent Grade) [RICCA] and water (HPLC grade) from Fisher; ethyl acetate (99.5%) and dichloromethane (99.5%, ACS Reagent Grade) from EMD Millipore; hexanes (ACS Reagent Grade) from Macron; ethanol (Reagent Grade) from Decon Laboratories; NO from Matheson Tri Gas; and CO2 from Airgas. Isopropyl nitrite was synthesized according to the procedure of Taylor et al. 15 and stored under vacuum until used.

Environmental Chamber Experiments. Reactions of 1tetradecene [CH₃(CH₂)₁₁CH=CH₂] and 1-pentadecene [CH₃(CH₂)₁₂CH=CH₂] with OH radicals in the presence of NO, were conducted in an ~7.4 m³ FEP Teflon environmental chamber that was flushed and filled with clean, dry air from two AADCO Model 737-14A clean air generators (<5 ppbv hydrocarbons, <0.1% relative humidity (RH)) and operated at room temperature (~25 °C) and atmospheric pressure (~630 Torr). The chamber volume was measured at the beginning of each experiment by adding a measured amount of CO₂ (prepared in a calibrated glass bulb on a vacuum manifold using a Baratron pressure gauge) in a flow of ultrahigh-purity (UHP) N2 and monitoring the concentration in the chamber with a GMT 220 Series CO₂ probe. Eight experiments were conducted: four with 1tetradecene and four with 1-pentadecene. For each experiment, the chamber was seeded with dioctyl phthalate (DOP) particles from an evaporation-condensation apparatus to achieve a mass concentration of \sim 250 μg m⁻³ as monitored by a scanning mobility particle sizer (SMPS).¹⁶ Then, 1 ppmv of either 1-tetradecene or 1-pentadecene was added from a heated glass bulb in a stream of UHP N₂, followed by 10 ppmv each of isopropyl nitrite and NO using the same procedure as used for the CO2. The chamber was mixed after adding each

component by running a Teflon-coated fan for 15 s. Blacklights located on two sides of the chamber, which have an emission spectrum (primarily from ca. 300-400 nm with a maximum at ~355 nm and a few discrete peaks at longer wavelengths) that overlaps well with the absorption spectrum of alkyl nitrites, 15 were then turned on to form OH radicals by photolysis of the isopropyl nitrite. To reven of the experiments the lights were on for 6 min at an intensity equivalent to a NO2 photolysis rate constant of 0.14 min⁻¹, and for one experiment they were on for 1 min at an intensity equivalent to a NO2 photolysis rate constant of 0.57 min⁻¹. About 50% of the 1-alkene reacted in each experiment and NO_{x1} which was monitored using a Thermo Environmental Instruments 42D NO-NO₂-NO_x analyzer, remained roughly constant. Aerosol mass concentrations increased in the first few minutes to 2500-3000 μ g m⁻³ as products condensed onto the seed aerosol.

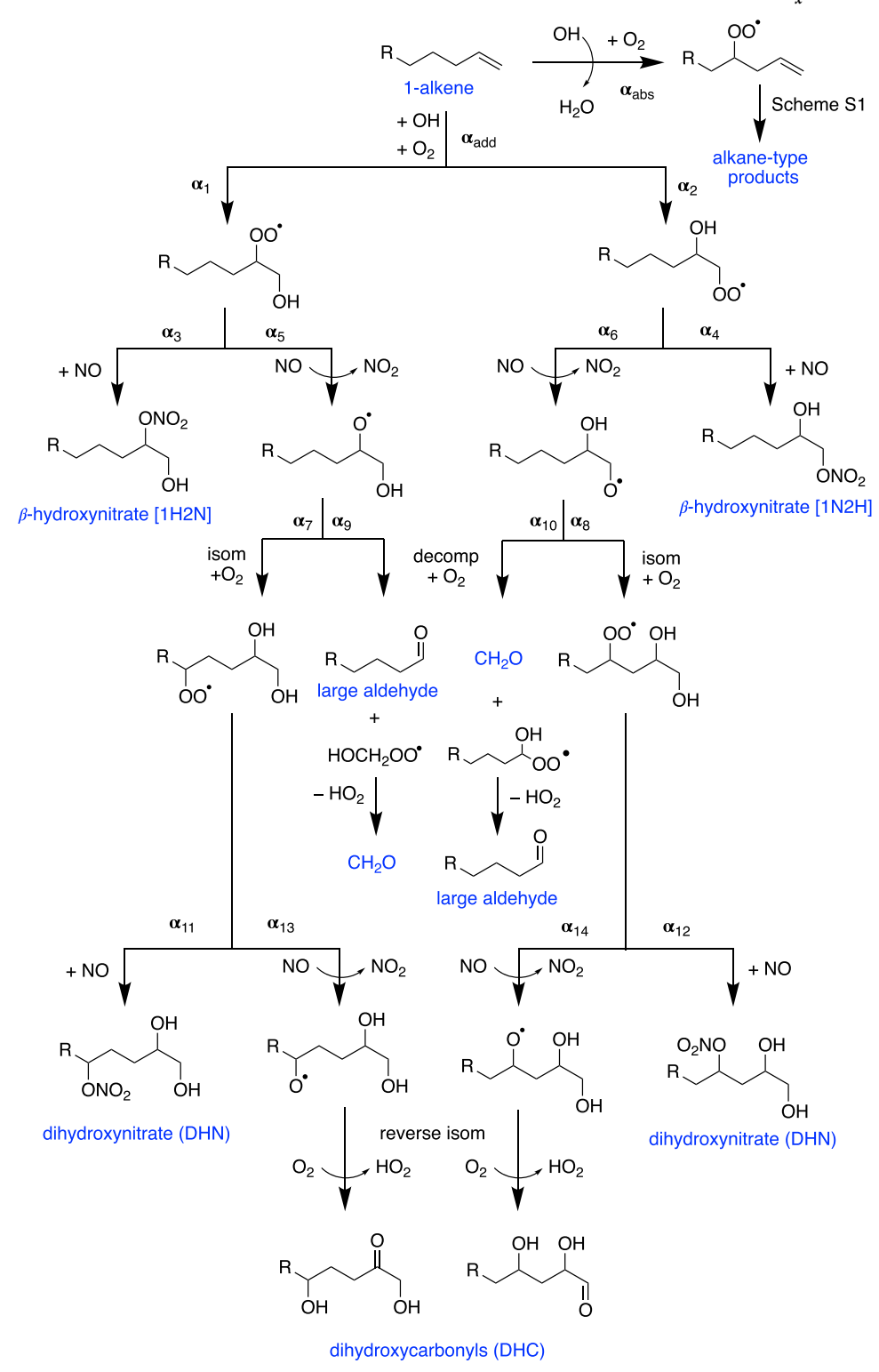
Gas-Phase Analysis. Gas-phase concentrations of 1-alkenes were measured by collecting three sequential 2-min samples of chamber air immediately before and after the reaction using glass tubes packed with Tenax solid adsorbent. Air was sampled at 250 cm³ min⁻¹ through a 10 cm long, 0.635 cm OD, 0.476 cm ID PFA Teflon tube that was first allowed to equilibrate with a flow of chamber air for 60 s, sufficient to prevent artifacts due to tubing wall losses.¹⁸ Tenax samples were analyzed by gas chromatography with flame ionization detection (GC-FID). The amount of 1-alkene reacted was determined using the equation from Yeh and Ziemann¹⁹

$$[Alk]_{reacted} = [Alk]_{T,i} \left(1 - \frac{FID_f}{FID_i}\right)$$
(1)

where $[Alk]_{T,i}$ is the amount of 1-tetradecene or 1-pentadecene initially added to the chamber divided by the chamber volume, and FID_i and FID_f are the FID peak areas measured before and after reaction, respectively. Tenax measurements made before and after the reactions agreed within $\pm 5\%$ and showed no consistent upward or downward trend, indicating that the C_{14} and C_{15} alkenes were essentially in equilibrium with the walls during sampling. This result is consistent with a previous experiment in which 1-tetradecene and 1-pentadecene reached gas-wall partitioning equilibrium in ~ 15 min, with 12 and 17% partitioned to the chamber walls, respectively. Therefore, the assumption that the 1-alkenes were in equilibrium with the walls during sampling seems appropriate, and the partitioning coefficient that would be used to correct the FID signals for gas-wall partitioning before and after the reaction cancels out in eq. 1.19

Gas-phase aldehydes (formaldehyde, tridecanal, and tetradecanal) were collected using cartridges and denuders. Cartridges packed with high-purity silica adsorbent and coated with 2,4-dinitrophenylhydrazine (2,4-DNPH), which selectively derivatizes carbonyls, were purchased from Sigma-Aldrich. Chamber air was sampled for 10 min at 650 cm³ min⁻¹ beginning 6 min after each 6-min reaction, and cartridges were extracted after 24 h with acetonitrile and analyzed by reversed-phase liquid chromatography using a Shimadzu model 20A HPLC outfitted with a Zorbax 5 μm XDB-C18 column and coupled to a UV-vis diode array detector. Formaldehyde-hydrazones were monitored at 360 nm and resolved using the acetonitrile/water complex gradient elution method of Karst et al.²¹ to avoid interference from 2,4dinitrophenylazide, the reaction product of NO2 with 2,4-DNPH. A time profile of the gradient elution method is shown

Scheme 1. Mechanism of the OH Radical Addition Reaction for 1-Alkenes in the Presence of NO.



in Figure S1. Formaldehyde was quantified by comparison to a synthesized formaldehyde-hydrazone standard prepared using California Air Resources Board Method 430,²² and formaldehyde yields were corrected for secondary reactions with OH radicals using an equation derived from the theory of consecutive reactions by Atkinson et al.²³

$$F = ((1 - k_{\text{HCHO}}/k_{\text{Alk}})(1 - ([\text{Alk}]_{t}/[\text{Alk}]_{o})) / (([\text{Alk}]_{t}/[\text{Alk}]_{o})^{k_{\text{HCHO}}/k_{\text{Alk}}} - ([\text{Alk}]_{t}/[\text{Alk}]_{o}))) - 1$$
(2)

where $k_{\rm HCHO}$ and $k_{\rm Alk}$ are the rate constants for the reactions of formaldehyde and 1-alkene with OH radicals, respectively, and [Alk]_t/[Alk]_o is the fraction of unreacted 1-alkene. Glass annular denuders purchased from URG Corporation were

coated with XAD-4 amberlite resin and additionally coated with O-(2,3,4,5,6-pentafluorobenzyl) hydroxylamine hydrochloride (PFBHA), which selectively derivatizes carbonyls. Chamber air was sampled onto denuders for 10 min at 10 L min⁻¹, beginning 40 min after each reaction to allow sufficient time to achieve gas-wall partitioning equilibrium. Denuders were then sealed and left in the dark at room temperature for 24 h, after which time they were extracted with dichloromethane (DCM) and analyzed by GC-FID.²⁴ Tridecanal and tetradecanal were quantified by comparison to synthesized tridecanal-oxime and tetradecanal-oxime standards prepared using the procedure of Yu et al.²⁵ In a separate experiment, 200 ppb each of C₅, C₆, C₁₃, and C₁₄ aldehydes were added to the chamber from a heated glass bulb, a fan was turned on for 15 s to mix the chamber, and the aldehydes were allowed to equilibrate will the walls for 40 min. Tenax samples were collected in the same way as during the other experiments, and peak areas for the four aldehydes were compared to the amount added to the chamber to determine the fraction that partitioned to the walls. The values for tridecanal and tetradecanal were 0.68 and 0.71, slightly higher than those measured previously for the corresponding 2-ketones^{26,27} because of their lower vapor pressures.

Particle-Phase Analysis. Aerosol was analyzed during reactions with a thermal desorption particle beam mass spectrometer (TDPBMS) to obtain real-time electron ionization mass spectra, and with an SMPS to measure aerosol size distributions and volume concentrations. Filter samples were collected before the reaction for 15 min and then after the 6-min reaction for 30 min at 14 L min⁻¹. Filters were immediately extracted three times with 4 mL of ethyl acetate for ≥10 min, and the extract was divided into two equal portions. The first portion was injected onto the HPLC and analyzed for nitrate-containing products. The eluent was monitored at 210 nm, where nitrate groups exhibit a strong absorption relative to the other functional groups present in the aerosol. The β -hydroxynitrate and dihydroxynitrate products were quantified by comparison to authentic standards synthesized by purifying an SOA extract from the 1tetradecene reaction using high-performance liquid chromatography (HPLC), and the 1,4-hydroxynitrates were quantified by comparison to a commercially available 2-ethylhexyl nitrate

The second portion of the SOA filter extract was derivatized in solution using DNPH according to the carbonyl functional group procedure described by Ranney and Ziemann.²⁸ Once derivatized, the extract was injected onto the HPLC and monitored at 360 nm (where singly derivatized compounds absorb strongly) and 430 nm (where doubly derivatized compounds absorb strongly).²⁹ Fractions were collected from the HPLC, concentrated into ~10 µL and injected onto a Thermo Scientific PolarisQ ion trap mass spectrometer using a direct insertion probe, with isobutane as the reagent gas. Particle-phase tridecanal and tetradecanal were quantified by comparison to a synthesized tridecanal-hydrozone standard prepared using the carbonyl functional group procedure,²⁸ and dihydroxycarbonyls were quantified by comparison to a surrogate standard, 6-hydroxy-5-decanone, which was chosen because it contains a hydroxyl group β to a carbonyl group, just like the dihydroxycarbonyl analytes. Calculations using gasparticle partitioning theory,³⁰ vapor pressures estimated using the SIMPOL.1 group contribution method,³¹ and measured aerosol mass concentrations of 2500-3000 μg m⁻³ indicate

that >99% of the β -hydroxynitrate, dihydroxynitrate, 1,4-hydroxynitrate, and dihydroxycarbonyl products were present in the particle phase. Therefore, we assume that the particle-phase yields for each product, excluding the aldehydes, are equal to the total yields.

Since gas-particle partitioning equilibrium is achieved within a few seconds for these aerosol mass concentrations, ²⁶ it can be assumed that partitioning of these products to the chamber walls (as gases) and secondary reactions with OH radicals was negligible. This assumption was tested by conducting an experiment in which the lights were turned on for 1 min but at a higher intensity (the amount of 1-alkene that reacted and amount SOA formed were similar to the 6-min reactions) so that the SOA mass concentration would increase more rapidly and thus enhance gas-to-particle partitioning and reduce gasto-wall partitioning and secondary OH radical reactions. Because no significant differences in the yields were observed between the 1-min and 6-min reactions, it appears that these potential product loss processes were negligible.

Particle-phase product yields were corrected for particle deposition to the walls using the nonvolatile DOP seed particles as an internal standard, where the correction factor was determined from the chamber concentrations of DOP measured on filters collected before and after reaction. The average particle wall loss for the 30-min post-reaction sampling period was ~5% (corresponding to an average correction factor of 1.05) for the eight experiments, similar to values of ca. $10-15\%\ h^{-1}$ measured previously for this chamber. Particle-phase product yields were not corrected for secondary reactions with OH radicals because our previous calculations for particle-phase β -hydroxynitrates²⁰ indicated that in these experiments only ~1% react with OH radicals.

■ RESULTS AND DISCUSSION

Reaction Mechanism. The mechanisms of the OH radical addition and H atom abstraction reactions for 1-alkenes in the presence of NO_x⁸⁻¹³ are shown in Schemes 1 and S1, respectively, where R and R' indicate alkyl groups. Branching ratios are labeled as α_i and are equal to the fraction of the reaction that proceeds by an indicated pathway. Hydroxyl radicals react with 1-alkenes either by abstracting an H atom from the carbon chain to form H_2O and an alkyl radical (α_{abs}) or by adding to the C=C bond ($\alpha_{\rm add}$) in either the 1-position (α_1) or the 2-position (α_2) to form a pair of β -hydroxyalkyl radicals. As the carbon chain length increases, the fraction of the reaction occurring by addition decreases. However, even for the large carbon numbers studied here (C_{14} and C_{15}), \sim 70% of the reaction occurs by addition to the C=C bond. For the OH radical addition pathway (Scheme 1), the β hydroxyalkyl radicals will add O2, and in the presence of NO will either add NO to form β -hydroxynitrates (α_3 , α_4), or NO will abstract an O atom to form NO_2 and the corresponding β hydroxyalkoxy radicals (α_5 , α_6). These radicals will either isomerize (α_7, α_8) by abstracting an H atom from further down the carbon chain (through a six-membered ring transition state) and then add O2 to form dihydroxyperoxy radicals, or decompose (α_9, α_{10}) to form more volatile aldehyde products (formaldehyde and a C_{13} or C_{14} aldehyde for the C_{14} and C_{15} 1-alkenes investigated here). The dihydroxyperoxy radicals can then react by the same pathways described above to form dihydroxynitrates (α_{11} , α_{12}) and dihydroxycarbonyls (α_{13} , α_{14}). For the H atom abstraction pathway, the mechanism and products are similar to those for the reactions of *n*-alkanes

Table 1. Measured Molar Yields of Products Formed by the OH Radical Addition Pathway in the Reactions of 1-Tetradecene (1-TD) and 1-Pentadecene (1-PD) in the Presence of NO_x (Schemes S1 and S2)

	molar yield		
product	1-TD	1-PD	average
1H2N β -hydroxynitrates	0.095 ± 0.01	0.092 ± 0.01	0.094 ± 0.01
1N2H β -hydroxynitrates	0.030 ± 0.003	0.032 ± 0.003	0.031 ± 0.003
dihydroxynitrates	0.052 ± 0.005	0.045 ± 0.004	0.048 ± 0.005
dihydroxycarbonyls	0.243 ± 0.05	0.237 ± 0.04	0.240 ± 0.04
formaldehyde	0.269 ± 0.02	0.259 ± 0.02	0.264 ± 0.02
C ₁₃ /C ₁₄ aldehyde (gas)	0.240 ± 0.03	0.260 ± 0.04	0.250 ± 0.04
C_{13}/C_{14} aldehyde (particle)	0.017 ± 0.003	0.025 ± 0.009	0.021 ± 0.008
C_{13}/C_{14} aldehyde (total)	0.257 ± 0.03	0.285 ± 0.04	0.271 ± 0.04
formaldehyde and C ₁₃ /C ₁₄ aldehyde (ave)	0.263 ± 0.03	0.272 ± 0.04	0.268 ± 0.03
OH radical addition (total)	0.683 ± 0.04	0.678 ± 0.05	0.681 ± 0.05

(Scheme S1): $^{33-35}$ the alkyl radical adds O_2 to form the corresponding alkylperoxy radical, which then reacts by mechanisms similar to those for β -hydroxyalkyl radicals to form alkyl nitrates, 1,4-hydroxynitrates, and 1,4-hydroxycarbonyls. The yields of these reaction products and the branching ratios involved in their formation have been previously measured. $^{19,33-35}$ We also note that although the various peroxy radicals formed can react with NO_2 to form peroxynitrates, they decompose reversibly within seconds and thus allow all peroxy radicals to eventually react with NO. And although the various alkoxy radicals formed can react with NO or NO_2 to form nitrates or nitrates, respectively, the reactions are too slow ($\ge 1 \times 10^{-4}$ s for $k = 4 \times 10^{-11}$ cm molecule $^{-1}$ s $^{-136}$ and [NO] and $[NO_2] \le 2 \times 10^{14}$ molecules cm $^{-3}$) to compete with decomposition and isomerization that occurs in $\sim 3 \times 10^{-6}$ s. 37

Measured Particle-Phase Yields of β -Hydroxynitrates, Dihydroxynitrates, and 1,4-Hydroxynitrates. The molar yields (moles of product formed/moles of alkene reacted) measured for all of the gas- and particle-phase products are given in Table 1. The reported uncertainties are standard deviations calculated across the eight experiments and correspond to relative uncertainties of ca. 10-40% with an average of ~15%. As shown in our previous detailed evaluation of the sources of error in measurements of the yields of the β hydroxynitrates,²⁰ these standard deviations are larger than the uncertainty obtained by propagating the errors contributed by all of the individual measurements and calculations used to determine the yield. The percent difference between the average C₁₄ and C₁₅ yields for each reaction product ranges from \sim 2 to \sim 30% with an average of \sim 9%, which falls within the experimental uncertainty.

A chromatogram showing the dihydroxynitrate, 1,4-hydroxynitrate, and β-hydroxynitrate reaction products is shown in Figure 1, where the β-hydroxynitrate and dihydroxynitrate peaks were assigned based on previous TDPBMS mass spectra and $^1\mathrm{H}$ NMR analysis. 10 The 1,4-hydroxynitrates were assigned here based on their absorbance at 210 nm (since no other organic nitrate products were expected in the particles) and the similar retention times to β-hydroxynitrates and dihydroxynitrates, which have similar structures. The particle-phase yields for the C_{14} and C_{15} β-hydroxynitrates and dihydroxynitrates were 0.125 \pm 0.01 (with isomer-specific yields of 0.094 \pm 0.01 for the 1H2N isomer and 0.031 \pm 0.003 for the 1N2H isomer) and 0.048 \pm 0.005, respectively. Isomer-specific yields for dihydroxynitrates were not determined because the isomers were not resolved on the HPLC.

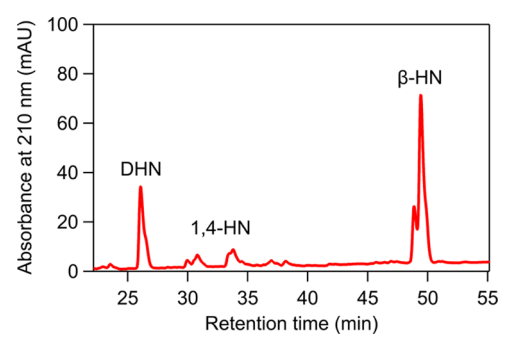


Figure 1. HPLC chromatogram of an extract of SOA formed from the reaction of 1-tetradecene with OH radicals in the presence of NO_x . The absorbance was monitored at 210 nm, where peaks correspond to the dihydroxynitrate (DHN), 1,4-hydroxynitrate (1,4-HN), and β-hydroxynitrate (β-HN) reaction products.

Dihydroxynitrates were measured previously for these reactions by Matsunaga and Ziemann¹⁰ with an average yield of 0.039. When corrected for losses due to the filter sampling method and for molar absorptivity,²⁰ this value becomes 0.039 \times 1.19 \times 1.06 = 0.049, in excellent agreement with the dihydroxynitrate yield measured in this work.

The particle-phase yield for the C_{14} and C_{15} 1,4-hydroxynitrate isomers (formed by the H atom abstraction pathway and seen as a series of peaks between 30 and 40 min on the chromatogram) was 0.036 ± 0.01 . This value is within ~25% of the value of 0.046 calculated from the fraction of reaction that occurred by H atom abstraction (0.30) and the 1,4-hydroxynitrate yield of 0.13 measured by Yeh and Ziemann³⁵ for reactions of C_{14} – C_{16} *n*-alkanes, corrected again by a factor of 1.19 for losses due to the filter sampling method.²⁰ The yields measured for each reaction product are reported in Table 1. There are no significant differences between the yields measured for the C_{14} and C_{15} 1-alkenes.

Calibration curves for the authentic dihydroxynitrate standard and the 2-ethylhexyl nitrate standard, which was used to quantify 1,4-hydroxynitrates, are shown in Figure S2A. During previous work, a pure mixture of C_{16} 1,4-hydroxynitrate isomers formed from the OH/NO $_x$ reaction of hexadecane was generated using the same HPLC fractionation method as for the dihydroxynitrates and yielded a calibration curve essentially identical to that of 2-ethylhexyl nitrate, as shown in Figure S2B. We note that, as discussed previously, 20 the authentic β -hydroxynitrate standard has a molar absorptivity (ε) lower than that of 2-ethylhexyl nitrate due to the influence of the β -hydroxyl group, where $\varepsilon_{\beta \rm HN} = 0.739 \times \varepsilon_{\rm EHN}$. For the authentic

dihydroxynitrate standard, the effect was larger, with $\varepsilon_{\rm DHN}=0.689\times\varepsilon_{\rm EHN}$. This was somewhat surprising, since the nearest hydroxyl group is farther from the UV-absorbing nitrate group in the dihydroxynitrate than the β -hydroxynitrate, and no effect of a similarly distant hydroxyl group was observed for the 1,4-hydroxynitrates. However, although it is well established that the presence of functional groups on carbons adjacent to the chromophore can alter the absorptivity, it has also been demonstrated that hydrogen bonding can shift absorption spectra and thus also have effects. 39

Measured Particle-Phase Yields of Dihydroxycarbonyls and Aldehydes. The remaining particle-phase reaction products did not contain a UV-absorbing nitrate group, and therefore could not be analyzed directly by HPLC-UV/vis. Instead, because they both contained a carbonyl group the SOA filter extracts were derivatized with DNPH prior to analysis by HPLC. The tridecanal and tetradecanal formed from the 1-tetradecene and 1-pentadecene reactions were quantified using derivatized commercially available standards, while dihydroxycarbonyls were quantified using a derivatized surrogate standard with a similar structure: 6-hydroxy-5decanone [CH₃(CH₂)₃CH(OH)C(O)(CH₂)₃CH₃]. When the 6-hydroxy-5-decanone was derivatized with DNPH and analyzed by HPLC to generate a standard curve, rather than a single peak for the corresponding hydrazone, the spectrum yielded three distinct peaks (Figure S3A). When the ratio of the absorbance at 430 nm to the absorbance at 360 nm was plotted (Figure S3B), it remained low (\sim 0.2) as the first two peaks eluted, and then increased to ~2 when the third peak eluted. According to work by Grosjean et al.,²⁹ this indicates that the third peak corresponds to a doubly derivatized reaction product. This was somewhat surprising, since the surrogate standard has only one carbonyl group, and the DNPH selectively reacts with carbonyls. However, this finding is also consistent with results from Grosjean et al., 29 who observed that DNPH derivatized both the carbonyl and hydroxyl groups in hydroxyacetaldehyde, a C_3 β -hydroxycarbonyl. CI-ITMS spectra of the three fractionated peaks confirmed that the first two peaks were isomers of the singly derivatized 6-hydroxy-5-decanone (Figure S4A,B), and the third peak was the doubly derivatized 6-hydroxy-5-decanone (Figure S4C).

The chromatogram for the DNPH-derivatized filter extract of SOA formed from the 1-pentadecene reaction is shown in Figure 2. The two sets of peaks at 56 and 58 min are assigned

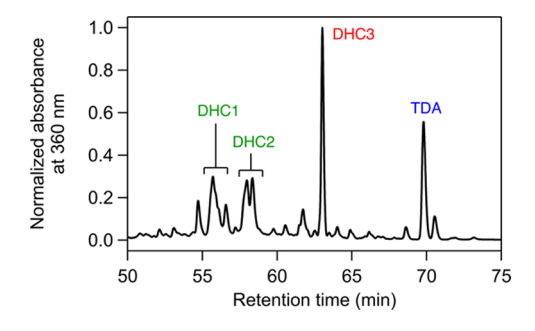


Figure 2. HPLC chromatogram of hydrazones in a DNPH-derivatized extract of SOA formed from the reaction of 1-pentadecene with OH radicals in the presence of NO_x. The absorbance was monitored at 360 nm, where the peaks correspond to isomers of the singly derivatized dihydroxycarbonyls (DHC1 and DHC2), the doubly derivatized dihydroxycarbonyls (DHC3), and tetradecanal (TDA).

as isomers of the singly derivatized C_{15} dihydroxycarbonyls (DHC1 and DHC2), and the peak at 63 min is assigned as the doubly derivatized C_{15} dihydroxycarbonyl (DHC3) based on the CI-ITMS mass spectra shown in Figure 3. The peaks

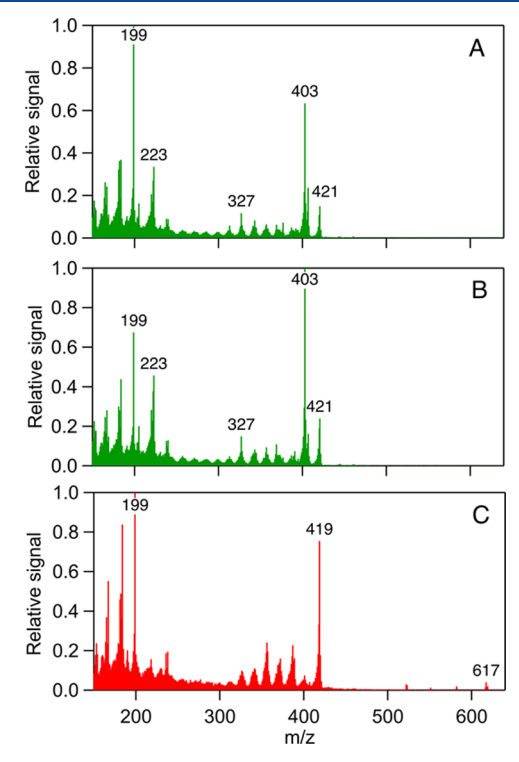


Figure 3. CI-ITMS mass spectra of fractionated hydrazones shown in Figure 2 for a DNPH-derivatized extract of SOA formed from the reaction 1-pentadecene with OH radicals in the presence of NO_x, obtained using isobutane as the reagent ion. Mass spectra in (A) and (B) correspond to the singly derivatized dihydroxycarbonyl isomers (DHC1 and DHC2, respectively), and in (C) to the doubly derivatized dihydroxycarbonyls (DHC3).

observed at m/z 421, 403, and 223 in Figure 3A,B correspond to ions formed by loss of H₂O, 2H₂O, and H₂O + DNPH from protonated singly derivatized C₁₅ dihydroxycarbonyl isomers; and the peaks observed at m/z 617 and 419 in panel 3C correspond to ions formed by loss of H_2 and H_2 + DNPH from the protonated doubly derivatized dihydroxycarbonyl. In all three mass spectra the peak at m/z 199 is from protonated DNPH. The peak in the chromatogram at 70 min is assigned to derivatized tetradecanal (TDA), based on the retention time of a derivatized tridecanal standard and the mass spectrum shown in Figure 4, which shows a large m/z 393 peak that corresponds to the protonated derivatized tridecanal. The other smaller peaks have not been identified but likely consist of 1,4-hydroxycarbonyl isomers formed from the H atom abstraction pathway or minor products of secondary reactions with OH radicals. Integrating these peaks and applying the calibration factor determined for tridecanal gives a total yield of ~ 0.10 .

The average particle-phase yields were 0.240 ± 0.04 for the C_{14} and C_{15} dihydroxycarbonyls and 0.021 ± 0.008 for the C_{13} and C_{14} aldehydes, as shown in Table 1. Although dihydroxycarbonyls have been shown to cyclize to form cyclic hemiacetals and to form trace amounts of oligomers, ¹⁴ the dihydroxycarbonyls present in those forms will be captured by the analysis since the acidic derivatization conditions cause the

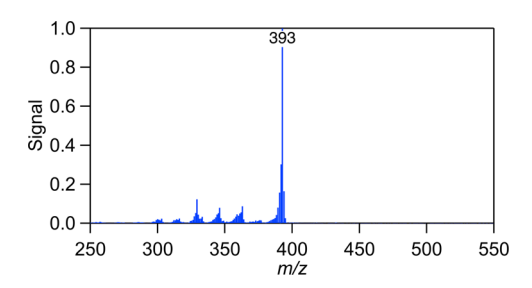


Figure 4. CI-ITMS mass spectrum of the fractionated tetradecanal (TDA) hydrazone shown in Figure 2 for a DNPH-derivatized extract of SOA formed from the reaction 1-pentadecene with OH radicals in the presence of NO_{xy} obtained using isobutane as the reagent ion.

oligomers and cyclic hemiacetals to dissociate. While the yields of dihydroxycarbonyls formed from reactions of 1-alkenes have not been accurately quantified previously, Kwok et al. estimated yields of dihydroxycarbonyls from the reactions of C_4 – C_8 1-alkenes by comparing the ratios of the signals attributed to the gas-phase dihydroxycarbonyl and aldehyde products in mass spectra measured using on-line atmospheric pressure ionization mass spectrometry (API-MS). The estimated yield for dihydroxycarbonyls formed from the largest 1-alkene, 1-octene, was 0.60, about twice the value measured here.

Measured Gas-Phase Yields of Aldehydes. The gasphase tridecanal and tetradecanal products were collected on PFBHA-coated denuders and the corresponding oximes were analyzed by GC-FID and quantified using synthesized authentic oxime standards. Formaldehyde, which was not observed in the gas chromatogram for the denuder samples, was instead collected and derivatized on DNPH cartridges and analyzed by HPLC. It is worth noting, however, that DNPH cartridges are difficult to employ in high-NO, experiments due to interference from the complex formed between NO₂ and the derivatizing agent. The HPLC chromatogram for a DNPH cartridge collected after a 1-tetradecene reaction is shown in Figure 5. The large peak at 4.4 min is from the reaction of NO₂ with the DNPH in the cartridge, which co-elutes with the formaldehyde-hydrazone when using simple solvent gradient methods. However, using the complex gradient elution shown in Figure S1, we were able to resolve and quantify the formaldehyde-hydrazone, which elutes at 6.2 min.

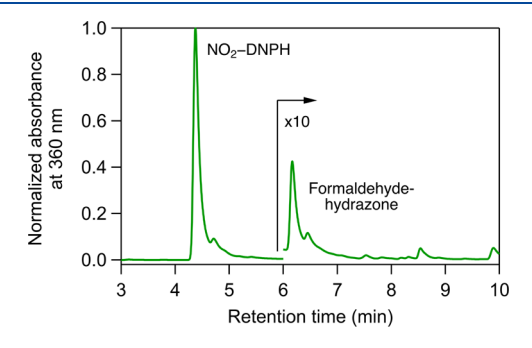


Figure 5. HPLC chromatogram of hydrazones in an extract from a DNPH cartridge used to collect and derivatize formaldehyde formed from the reaction 1-pentadecene with OH radicals in the presence of NO_x . The absorbance was monitored at 360 nm, where the reaction product of NO_2 with DNPH elutes at 4.4 min and the formaldehydehydrazone at 6.2 min. Absorbances at 6 min and beyond have been multiplied by 10.

The formaldehyde yields determined from these measurements were corrected for secondary reactions with OH radicals using consecutive reaction rate theory²³ and the rate constants for the reactions of formaldehyde⁴⁰ and the 1-alkene precursors³² with OH radicals of 9.4×10^{-12} , 5.2×10^{-11} , and 5.3×10^{-11} cm³ molecules⁻¹ s⁻¹, respectively, which resulted in a loss of 7% of formaldehyde. No corrections were made for gas-wall partitioning, which should not occur for formaldehyde because of its high vapor pressure.

The tridecanal and tetradecanal yields were corrected for both secondary reactions with OH radicals and gas-wall partitioning using a kinetics model written in KinSim. 41 The rate constants for reaction of OH radicals with these aldehydes were calculated to be 3.7×10^{-11} and 3.9×10^{-11} cm³ molecules⁻¹ s⁻¹, respectively, using structure—activity relationships, 42 and the average concentration of OH radicals was calculated to be 3.7×10^7 molecules cm⁻³ using the fraction of unreacted 1-alkene and the OH radical rate constants for 1alkenes given above. The rate constants for partitioning to and from the walls were calculated to be 8.7×10^{-4} and 4.1×10^{-4} s^{-1} for tridecanal and 9.2 \times 10^{-4} and 3.6 \times 10^{-4} s^{-1} for tetradecanal using equations given in Matsunaga and Ziemann, 26 a gas-wall equilibration timescale of 13 min based on recent experiments conducted with 2-ketones,⁴ and the ratio of the concentrations of aldehyde in the gas phase and in the walls per chamber volume at equilibrium of 0.47 and 0.39 for tridecanal and tetradecanal, respectively, determined as described above. First, the model was run without gas-wall partitioning, and the calculated fraction of aldehyde formed that was lost to secondary reactions with OH radicals alone was 0.291, in agreement with the value calculated using consecutive reaction rate theory (eq 2). However, because the aldehydes simultaneously partitioned to the chamber walls, where they would not be available to react with OH radicals, this value overestimates the loss by reactions. Gas-wall partitioning was then incorporated into the model and the aldehyde yield was adjusted until the predicted concentration in the chamber during sampling agreed with the measured value. The value of ([ald] $_{gas}$ + [ald] $_{walls}$)/[ald] $_{gas}$ of 3.72 calculated from the model was then multiplied by the measured value of [ald]gas and divided by the measured concentration of 1-alkene reacted to determine the corrected aldehyde yield of 0.250. Most of the yield correction was due to gas-wall partitioning, since ~70% of the aldehyde partitioned to the walls in the experiments described above.

We note that measured partitioning of aldehydes compares reasonably well with predictions from gas-particle³⁰ and gas-wall²⁶ partitioning theory. Using aldehyde vapor pressures calculated with SIMPOL.1,³¹ a typical measured particle mass concentration of 3 mg m⁻³, and an assumed effective wall mass concentration similar to ketones of 25 mg m⁻³,⁴³ the average fractions of C_{13} and C_{14} aldehydes in the gas phase, particles, and walls are predicted to be 0.54, 0.05, and 0.41, compared to measured average values of 0.25, 0.08, and 0.67, respectively.

The resulting gas-phase yields were 0.264 ± 0.02 for formaldehyde and 0.250 ± 0.04 for the C_{13} and C_{14} aldehydes, with the total yield of the large aldehydes being 0.271 ± 0.04 (0.250 ± 0.04 for the gas phase and 0.021 ± 0.008 for the particle phase). As shown in Scheme 1, formaldehyde and the C_{13} or C_{14} aldehyde should have the same molar yields. But in a study of the reaction of 1-octene, Aschmann et al. howed that the RCH₂CH₂C(OH)OO• radical can also react with NO before it decomposes, leading to the formation of formic acid

and a C₆ alkyl radical (which reacted to form a C₆ 1,4hydroxyaldehyde with a yield of 0.04, and other unmeasured products), and thus a reduction in the yield of the large aldehyde (heptanal) relative to formaldehyde. Here, the measured yield of the large aldehyde is slightly larger than that of formaldehyde, but the level of agreement gives confidence that the values are reasonably accurate. Furthermore, the large aldehyde yield of 0.271 ± 0.04 agrees well with the heptanal yield of 0.28 ± 0.03 reported by Aschmann et al., 11 although both of these (and the formaldehyde yield measured here of 0.264 \pm 0.02) are smaller than the formaldehyde yield of 0.39 ± 0.06 measured earlier for the 1-octene reaction by the same co-workers using gas chromatography and in situ Fourier transform infrared spectroscopy.8 When comparing the results of their two studies, Aschmann et al. 11 conclude that the yields of formaldehyde (0.39) and the sum of the measured yields of heptanal and the C_6 1,4-hydroxyaldehyde (0.28 + 0.04 = 0.32) are within their measurement uncertainties. As discussed in the following section, if the other products expected from the C₆ alkyl radical are also included in this estimate then the sum of the heptanal and C_6 product yields should be ~0.35. It is also likely that some of the excess formaldehyde observed for the 1octene reaction is due to secondary reactions in which firstgeneration H atom abstraction products react by OH radical addition, which will lead in part to formaldehyde and C7 multifunctional aldehyde co-products. These secondary reactions would be less important in our experiments, since most of the H atom abstraction products will partition to particles, where OH radical reactions are negligible.

Based on this discussion, it seems likely that the formaldehyde yields measured here should be somewhat larger than those measured for the large aldehydes. The reason they are not could be due to an overestimate in the correction of the large aldehyde yields for gas-wall partitioning, although this was well characterized from measurements and the corrected large aldehyde yields are essentially the same as the heptanal yield measured by Aschmann et al. It is also possible that the formaldehyde yields are slightly underestimated due to the sample collection and analysis methods. The possible consequences of this discrepancy for our results are evaluated below, where we use an average of the yields measured for formaldehyde and the large aldehydes, 0.268 \pm 0.03, in mass balance calculations.

Mass Balance Comparison of Product Yields. Having measured molar yields for each of the major reaction products for the addition pathway of the reactions of the C₁₄ and C₁₅ 1alkenes, we can compare the sum of the yields with the value expected from the average branching ratio for OH radical addition, $\alpha_{\rm add} = (0.69 + 0.71)/2 = 0.70$. Table 1 shows the average molar yields for each reaction product and their sum, 0.681 ± 0.05 . The excellent agreement suggests that the reaction mechanism quantitatively captures most of the products formed in these reactions. As discussed above, however, Aschmann et al. 11 showed that the large α hydroxyperoxy radical formed by addition of O_2 to the α hydroxyalkyl radical co-product of formaldehyde can react with NO by O atom abstraction, in addition to decomposing to form a large aldehyde (Scheme 1) and HO_2 . The resulting α hydroxyalkoxy radical subsequently decomposes to formic acid and an alkyl radical, which can react to form a 1,4hydroxyaldehyde and other products. While the 1,4-hydroxyaldehyde product could not be identified in this work, using

the 1,4-hydroxyaldehyde yield of 0.04 measured by Aschmann et al.11 and assuming that an alkyl nitrate and 1,4hydroxynitrate are also formed from the alkyl radical in accordance with the mechanism and branching ratios shown in Scheme S3, the total yield of products formed by this pathway would be 0.07. If similar yields of these products were formed here it would increase the total measured yield from 0.68. to 0.75, a value that is \sim 7% higher than the expected value of 0.70 but within uncertainties of both measurements. We note that the yields of alkyl nitrates, 1,4-hydroxynitrates, and 1,4hydroxycarbonyls expected to be formed by H atom abstraction (Scheme S1) are 0.09, 0.05, and 0.16, respectively, based on the corresponding yields of 0.29, 0.16, and 0.55 for the reactions of n-alkanes. ^{19,35} In these calculations, the measured 1,4-hydroxynitrate yield of 0.1335 was multiplied by a factor or 1.19 to correct for losses due to the filter sampling method as described above,²⁰ which also slightly reduced the 1,4-hydroxycarbonyl yield of 0.58 that was calculated by difference.33

Calculation of Branching Ratios for OH Radical **Addition Pathways.** Because the molar yield of a reaction product is equal to the product of the branching ratios along the pathway leading to that product, we can use the values of the branching ratios $\alpha_{\rm add} = 0.70$ and $\alpha_{\rm abs} = 0.30$ determined from kinetics measurements,³² the values of $\alpha_1 - \alpha_6$ of 0.74, 0.26, 0.18, 0.17, 0.82, and 0.83 we determined previously, and the yields of dihydroxycarbonyls, dihydroxynitrates, and aldehydes measured here to quantify the branching ratios $\alpha_7 - \alpha_{14}$ shown in Scheme 1. Since decomposition of the two β hydroxyalkoxy radical isomers leads to the same products (formaldehyde and a large aldehyde), making the two pathways indistinguishable, we assume that $\alpha_{\text{isom}} = \alpha_7 = \alpha_8$ and $\alpha_{dec} = \alpha_9 = \alpha_{10}$. Then, using our average C_{13} and C_{14} aldehyde/formaldehyde yield of 0.268 and $\alpha_{\rm dec}$ = $Y_{\rm ald}/[(\alpha_{\rm add} \times$ $\alpha_1 \times \alpha_5$) + $(\alpha_{\rm add} \times \alpha_2 \times \alpha_6)$], we calculate $\alpha_{\rm dec} = 0.47$ for the decomposition of β -hydroxyalkoxy radicals and $\alpha_{\rm isom}$ = $1-\alpha_{\rm dec}$ = 0.53. These values are similar to those measured previously for β -hydroxyalkoxy radicals formed from 1-octene, 11 0.42 and 0.58, but very different from values of 0.94 and 0.06 estimated from structure-activity relationships 44,45 that predict nearly complete decomposition. Assuming also that $\alpha_{\rm DHN}$ = α_{11} = α_{12} and $\alpha_{\rm DHC} = \alpha_{13} = \alpha_{14}$, since we cannot distinguish the dihydroxynitrate (DHN) or dihydroxycarbonyl (DHC) isomers formed from the two pathways, we use the measured yields of dihydroxynitrates and dihydroxycarbonyls to calculate $\alpha_{\rm DHN}$ and $\alpha_{\rm DHC}$ in two ways: $\alpha_{\rm DHN} = Y_{\rm DHN} / [(\alpha_{\rm add} \times \alpha_1 \times \alpha_5 \times \alpha_5$ α_7) + $(\alpha_{\rm add} \times \alpha_2 \times \alpha_6 \times \alpha_8)$] and $\alpha_{\rm DHC} = 1 - \alpha_{\rm DHN}$, $\alpha_{\rm DHC} =$ $Y_{\rm DHC}/[(\alpha_{\rm add} \times \alpha_1 \times \alpha_5 \times \alpha_7) + (\alpha_{\rm add} \times \alpha_2 \times \alpha_6 \times \alpha_8)]$ and $\alpha_{\rm DHN}$ = 1 - $\alpha_{\rm DHC}$. The values of $\alpha_{\rm DHN}$ and $\alpha_{\rm DHC}$ calculated from the 0.048 yield of dihydroxynitrates are 0.16 and 0.84, and those calculated from the 0.240 yield of dihydroxycarbonyls are 0.21 and 0.79, giving averages of 0.19 \pm 0.03 and 0.81 ± 0.03 . The branching ratio for dihydroxynitrate formation is essentially the same as the value of 0.18 for the formation of secondary β -hydroxynitrates, providing further evidence that hydrogen bonding with a hydroxyl group reduces the strength of the O-O bond in hydroxyperoxy radical-NO complexes, thus reducing the branching ratio for organic nitrate formation compared to alkylperoxy radicals.46 The average calculated branching ratios for C₁₄ and C₁₅ 1-alkenes for the OH radical addition pathways are shown in Scheme S2, which have been added to the reaction mechanism in Scheme 1. Measured branching ratios for the H atom abstraction pathway are shown in Scheme S3, where they have been added to the Scheme S1 reaction mechanism. There the value of 0.29 for alkyl nitrate formation was taken from Yeh and Ziemann, 19 the value of 0.22 for 1,4-hydroxynitrate formation was taken from Yeh and Ziemann³⁵ and multiplied by a factor or 1.19 to correct for losses due to the filter sampling method as described above,²⁰ and the value for 1,4-hydroxycarbonyl formation was calculated as 1-0.22 = 0.78.

Branching Ratios and Product Yields for OH Radical Addition and H Atom Abstraction Pathways for C₅-C₁₅ 1-Alkenes. The branching ratios in Scheme 1 calculated above for the plateau region of 1-alkene carbon numbers $\geq C_{14}$ and shown in Scheme S2 can be extrapolated to smaller carbon numbers as follows: (a) use the equations from Nishino et al.³² to calculate the fraction of OH reaction that occurs by addition to the C=C bond (α_{add}) and H atom abstraction (α_{abs}) ; (b) assume the branching ratios for OH radical addition to the C=C bond (α_1 = 0.74 and α_2 = 0.26) are independent of carbon number; (c) use the model of Arey et al.³³ to account for the effect of carbon number on the branching ratios for the reactions of β -hydroxyperoxy (α_3 - α_6) and dihydroxyperoxy $(\alpha_{11}-\alpha_{14})$ radicals with NO (see Bakker-Arkema and Ziemann²⁰ for an example of this approach); and (d) use the yields of 0.73, 0.46, 0.30, and 0.28 measured by Atkinson et al.8 and Aschmann et al.11 for butanal, pentanal, hexanal, and heptanal formed from the same reactions of C₅-C₈ 1-alkenes and the equations above to calculate the branching ratios for decomposition and isomerization of β -hydroxyalkoxy radicals $(\alpha_7 - \alpha_{10})$. For the H atom abstraction pathway, all that is needed is to use the model of Arey et al.³³ to account for the effect of carbon number on the branching ratios for the reactions of unsaturated alkylperoxy ($lpha_{15}$, $lpha_{16}$) and 1,4hydroxyperoxy (α_{17} , α_{18}) radicals with NO, since these are the only branching ratios in the mechanism (Schemes S1 and

The results of the branching ratio calculations for the OH radical addition pathways are shown in Figure 6. As the carbon

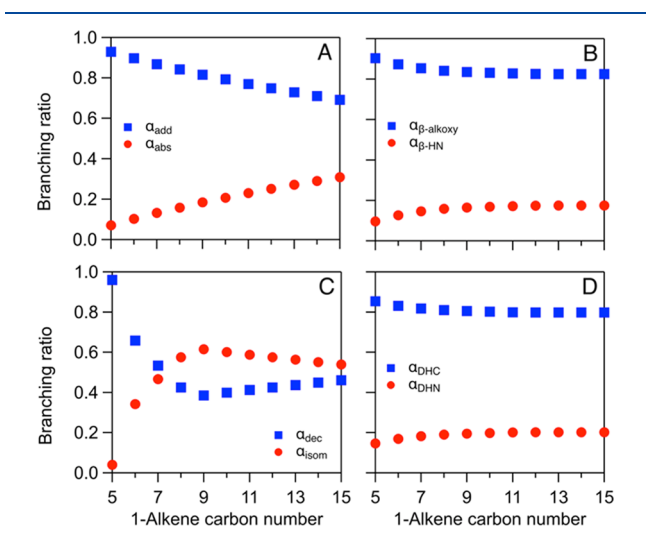


Figure 6. Modeled carbon number dependence of the branching ratios for (A) OH radical addition and H atom abstraction, (B) β alkoxy radical and β -hydroxynitrate formation, (C) β -alkoxy radical decomposition and isomerization, and (D) dihydroxycarbonyl and dihydroxynitrate formation, in the mechanism of the reaction of 1alkenes with OH radicals in the presence of NO_x (Schemes S1 and

number increases the branching ratio for OH radical addition decreases while that for H atom abstraction increases because of the increased number of abstractable H atoms on a longer carbon chain (Figure 6A). Branching ratios for the formation of β -hydroxynitrates and dihydroxynitrates both increase with increasing carbon number, while those for the corresponding β-hydroxyalkoxy and dihydroxyalkoxy radicals decrease (Figure 6B,D) because a higher carbon number increases the number of vibrational modes over which the reaction exothermicity can be distributed in the β -hydroxyperoxy-NO and dihydroxyperoxy-NO intermediates, allowing more time for rearrangement to the organic nitrate. 47 The branching ratios for decomposition and isomerization of β -hydroxyalkoxy radicals depend strongly on carbon number, with values of ~ 0 and ~ 1 at C_5 that increase and decrease to \sim 0.6 and \sim 0.4 at C₉, respectively, before both approaching \sim 0.5 at C₁₅. This trend is similar to what we observed previously for the same reactions of 2methyl-1-alkenes, 13 although in that case a clear plateau was reached for both values at C_9 (0.49 and 0.51 for decomposition and isomerization) rather than maxima and minima. This difference may be due to the absence of aldehyde yield data for the C_9-C_{13} 1-alkenes, resulting in poorer model constraints compared to the 2-methyl-1-alkenes, where 2-ketone yields were measured for C_6-C_{13} . Furthermore, because the branching ratios for decomposition and isomerization are inversely related, this plot exaggerates the differences in the curves, which each only change by $\sim 10\%$ between C_9 and C_{15} . Assuming then that the branching ratios are similar from C₈-C₁₅ (as noted above, the measured values were 0.47 and 0.53 here and 0.42 and 0.58 previously, respectively), 11 it is interesting that for both the 1-alkenes and 2-methyl-1-alkenes, the branching ratios begin to differ from plateau values when the alkyl chain length decreases to C₅ (carbon number C₇ for 1-alkenes and C_8 for 2-methyl-1-alkenes). As discussed previously, 13 the reason that branching ratios for decomposition and isomerization are ~0 and ~1 for a C3 alkyl chain is because isomerization of the dominant 1-hydroxy-2-alkoxy radical via a 1,5-H-shift involves abstraction of a primary H atom from the terminal methyl group, which is energetically unfavorable and allows decomposition to dominate. The changes in branching ratios that occur as the alkyl chain is lengthened are then likely due to the greater ease of abstracting secondary H atoms and possibly the reduced effects of chemical activation on the rate of decomposition because of the larger number of vibrational modes available to accommodate the reaction exothermicity before the β hydroxyalkoxy radical can be thermalized by collisions.

The modeled yields of the products of both the OH radical addition and H atom abstraction pathways are shown in Figure 7. Yields for the alkyl nitrate, 1,4-hydroxynitrate, and 1,4hydroxycarbonyl H atom abstraction products all increase monotonically with increasing carbon number because of the increase in the fraction of OH reaction that occurs by H atom abstraction (Figure 6A). The yields of the β -hydroxynitrate and dihydroxynitrate products formed by OH radical addition also increase with increasing carbon number, but they reach a plateau at C₈-C₁₀ before decreasing. The initial increase is due to an increase in the branching ratios for organic nitrate formation (Figure 6B), but as they approach their plateaus at higher carbon numbers the effect of the decreasing fraction of reaction that occurs by OH radical addition (Figure 6A) becomes dominant and the yields decrease. Yields for the aldehydes and dihydroxycarbonyls behave quite differently

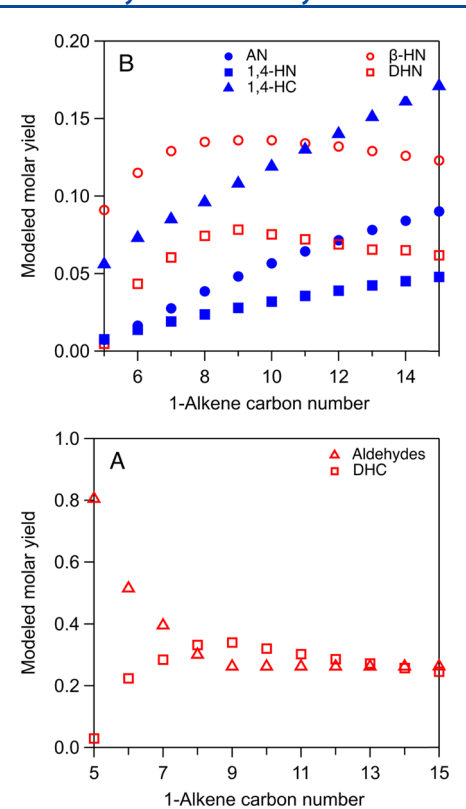


Figure 7. Modeled carbon number dependence of the yields of (A) alkyl nitrate, 1,4-hydroxynitrate, 1,4-hydroxynitrate, dihydroxynitrate, and (B) aldehyde and dihydroxycarbonyl products of the reaction of 1-alkenes with OH radicals in the presence of NO_x (Schemes 1 and S1–S3).

from all of the other products because of the inverse relationship in the branching ratios for their formation (Figure 6C).

CONCLUSIONS

Large numbers of laboratory studies have been conducted to determine the gas- and particle-phase products formed from the oxidation of anthropogenic and biogenic VOCs to better understand the atmospheric fate of VOCs and their impact on O₃ and SOA formation. In most cases, only a modest fraction of the products was identified and quantified, in large part because of the complexity of many VOC oxidation reactions and the limitations of analytical methods. Here, we have demonstrated that by combining gas and particle sample collection with offline derivatization, gas and liquid chromatography, and mass spectrometry methods, nearly all of the products formed from the OH radical addition to 1-alkenes in the presence of NOx could be identified and quantified such that essentially a complete mass balance could be obtained for the \sim 70% of products that are expected to be formed by this pathway. When combined with yields of products measured previously for the reaction of n-alkanes under similar conditions, which are expected to be the same as those formed by the H atom abstraction pathway that leads to the other 30% of products, a very complete, quantitative understanding of the reaction mechanism is achieved. Although use of these methods might not be as successful for analyses of much more complex product mixtures, the branching ratios measured for fundamental reaction pathways such as OH radical addition to C=C bonds, reactions of NO

with hydroxyperoxy radicals, and isomerization and decomposition of hydroxyalkoxy radicals, reported here over a large range of carbon numbers by combining measurements and modeling, may be useful in developing reaction mechanisms for more complex reactions. Such mechanisms might then be incorporated into box models used to interpret results of laboratory studies or into chemical transport models used to simulate atmospheric chemical and physical processes.

ASSOCIATED CONTENT

5 Supporting Information

The Supporting Information is available free of charge at https://pubs.acs.org/doi/10.1021/acs.jpca.1c03688.

Schemes for the mechanisms of H atom abstraction (without and with values of branching ratios) and for OH radical addition (with values of branching ratios) for reactions of 1-alkenes with OH radicals in the presence of NO_x ; complex gradient elution method from Karst et al.,²¹ HPLC calibration curves for 2-ethylhexyl nitrate and authentic dihydroxynitrate and 1,4-hydroxynitrate standards, HPLC chromatogram for derivatized 6-hydroxy-5-decanone and the corresponding absorbance ratio (430 nm/360 nm), CI-ITMS mass spectra of 6-hydroxy-5-decanone hydrazones; and a table listing the reactions and rate constants used in the KinSim model to correct measured C_{13} and C_{14} aldehyde yields for gaswall partitioning and secondary reactions with OH radicals (PDF)

AUTHOR INFORMATION

Corresponding Author

Paul J. Ziemann — Department of Chemistry, University of Colorado, Boulder, Colorado 80309, United States; Cooperative Institute for Research in Environmental Sciences (CIRES), Boulder, Colorado 80309, United States; orcid.org/0000-0001-7419-0044; Phone: 303-492-9654; Email: paul.ziemann@colorado.edu

Author

Julia G. Bakker-Arkema — Department of Chemistry, University of Colorado, Boulder, Colorado 80309, United States; Cooperative Institute for Research in Environmental Sciences (CIRES), Boulder, Colorado 80309, United States; orcid.org/0000-0002-3120-6058

Complete contact information is available at: https://pubs.acs.org/10.1021/acs.jpca.1c03688

Note

The authors declare no competing financial interest.

ACKNOWLEDGMENTS

This material is based on work supported by the National Science Foundation (NSF) under grants AGS-1420007 and AGS-1750447. The authors also thank Lucas Algrim for the use of his measured 1,4-hydroxynitrate and 2-ethylhexyl nitrate calibration curves.

REFERENCES

(1) Hallquist, M.; Wenger, J. C.; Baltensperger, U.; Rudich, Y.; Simpson, D.; Claeys, M.; Dommen, J.; Donahue, N. M.; George, C.; Goldstein, A. H.; et al. The Formation, Properties, and Impact of

- Secondary Organic Aerosol: Current and Emerging Issues. Atmos. Chem. Phys. 2009, 9, 5155-5236.
- (2) Pöschl, U. Atmospheric Aerosols: Composition, Transformation, Climate and Health Effects. *Angew. Chem., Int. Ed.* **2005**, 44, 7520–7540
- (3) Wennberg, P. O.; Bates, K. H.; Crounse, J. D.; Dodson, L. G.; McVay, R. C.; Mertens, L. A.; Nguyen, T. B.; Praske, E.; Schwantes, R. H.; Smarte.; et al. Gas-Phase Reactions of Isoprene and its Major Oxidation Products. *Chem. Rev.* **2018**, *118*, 3337–3390.
- (4) Claflin, M. S.; Ziemann, P. J. Identification and Quantitation of Aerosol Products of the Reaction of β -Pinene with NO₃ Radicals and Implications for Gas- and Particle-Phase Reaction Mechanisms. *J. Phys. Chem. A* **2018**, *122*, 3640–3652.
- (5) Guenther, A. B.; Jiang, X.; Heald, C. L.; Sakulyanontvittaya, T.; Duhl, T.; Emmons, L. K.; Wang, X. The Model of Emissions of Gases and Aerosols from Nature Version 2.1 (MEGAN2.1): An Extended and Updated Framework for Modeling Biogenic Emissions. *Geosci. Model Dev.* 2012, 5, 1471–1492.
- (6) Johnson, D.; Utembe, S. R.; Jenkin, M. E. Simulating the Detailed Chemical Composition of Secondary Organic Aerosol Formed on a Regional Scale during the TORCH 2003 Campaign in the Southern UK. Atmos. Chem. Phys. 2006, 6, 419–431.
- (7) May, A. A.; Nguyen, N. T.; Presto, A. A.; Gordon, T. D.; Lipsky, E. M.; Karve, M.; Gutierrez, A.; Robertson, W. H.; Zhang, M.; Brandow, C.; et al. Gas- and Particle-Phase Primary Emissions from In-Use, On-Road Gasoline and Diesel Vehicles. *Atmos. Environ.* **2014**, 88, 247–260.
- (8) Atkinson, R.; Tuazon, E. C.; Aschmann, S. M. Products of the Gas-Phase Reactions of a Series of 1-Alkenes and 1-Methylcyclohexene with the OH Radical in the Presence of NO. *Environ. Sci. Technol.* **1995**, 29, 1674–1680.
- (9) Kwok, E. S. C.; Atkinson, R.; Arey, J. Isomerization of β-Hydroxyalkoxy Radicals Formed from the OH Radical-Initiated Reactions of C₄-C₈ 1-Alkenes. *Environ. Sci. Technol.* **1996**, 30, 1048–1052.
- (10) Matsunaga, A.; Ziemann, P. J. Yields of β -Hydroxynitrates and Dihydroxynitrates in Aerosol Formed from OH Radical-Initiated Reactions of Linear Alkenes in the Presence of NO_x. *J. Phys. Chem. A* **2009**, *113*, 599–606.
- (11) Aschmann, S. M.; Tuazon, E. C.; Arey, J.; Atkinson, R. Products and Mechanisms of the Gas-Phase Reactions of OH Radicals with 1-Octene and 7-Tetradecene in the Presence of NO. *Environ. Sci. Technol.* **2010**, *44*, 3825–3831.
- (12) Matsunaga, A.; Ziemann, P. J. Yields of β -Hydroxynitrates, Dihydroxynitrates, and Trihydroxynitrates Formed from OH Radical-Initiated Reactions of 2-Methyl-1-Alkenes. *Proc. Natl. Acad. Sci. U.S.A.* **2010**, *107*, 6664–6669.
- (13) Matsunaga, A.; Ziemann, P. J. Branching Ratios and Rate Constants for Decomposition and Isomerization of β -Hydroxyalkoxy Radicals Formed from OH Radical-Initiated Reactions of C_6-C_{13} 2-Methyl-1-Alkenes in the Presence of NO_x. J. Phys. Chem. A **2019**, 123, 7839–7846.
- (14) Matsunaga, A.; Docherty, K. S.; Lim, Y. B.; Ziemann, P. J. Composition and Yields of Secondary Organic Aerosol Formed from OH Radical-Initiated Reactions of Linear Alkenes in the Presence of NO_x: Modeling and Measurements. *Atmos. Environ.* **2009**, 43, 1349–1357.
- (15) Taylor, W. D.; Allston, T. D.; Moscato, M. J.; Fazekas, G. B.; Kozlowski, R.; Takacs, G. A. Atmospheric Photodissociation Lifetimes for Nitromethane, Methyl Nitrite, and Methyl Nitrate. *Int. J. Chem. Kinet.* **1980**, 12, 231–240.
- (16) Docherty, K. S.; Ziemann, P. J. Reaction of Oleic Acid Particles with NO₃ Radicals: Products, Mechanism, and Implications for Radical-Initiated Organic Aerosol Oxidation. *J. Phys. Chem. A* **2006**, *110*, 3567–3577.
- (17) Atkinson, R.; Carter, W. P. L.; Winer, A. M.; Pitts, J. N. An Experimental Protocol for the Determination of OH Radical Rate Constants with Organics using Methyl Nitrite Photolysis as an OH Radical Source. *J. Air Pollut. Control Assoc.* 1981, 31, 1090–1092.

- (18) Pagonis, D.; Krechmer, J. E.; de Gouw, J.; Jimenez, J. L.; Ziemann, P. J. Effects of Gas-Wall Partitioning in Teflon Tubing and Instrumentation on Time-Resolved Measurements of Gas-Phase Organic Compounds. *Atmos. Meas. Tech.* **2017**, *10*, 4687–4696.
- (19) Yeh, G. K.; Ziemann, P. J. Alkyl Nitrate Formation from the Reactions of C_8-C_{14} *n*-Alkanes with OH Radicals in the Presence of NO_x : Measured Yields with Essential Corrections for Gas–Wall Partitioning. *J. Phys. Chem. A* **2014**, *118*, 8147–8157.
- (20) Bakker-Arkema, J. G.; Ziemann, P. J. Minimizing Error in Measured Yields of Particle-Phase Products formed in Environmental Chamber Reactions: Revisiting the Yields of β -Hydroxynitrates Formed from 1-Alkene + OH/NO_x Reactions. ACS Earth Space Chem. **2021**, *5*, 690–702.
- (21) Karst, U.; Binding, N.; Cammann, K.; Witting, U. Interferences of Nitrogen Dioxide in the Determination of Aldehydes and Ketones by Sampling on 2,4-Dinitrophenylhydrazine-Coated Solid Sorbent. *Fresenius' J. Anal. Chem.* **1993**, 345, 48–52.
- (22) Air Resources Board Method 430. Determination of Formaldehyde and Acetaldehyde in Emissions from Stationary Sources. California Environmental Protection Agency: Sacramento, 1991.
- (23) Atkinson, R.; Aschmann, S. M.; Carter, W. P. L.; Winer, A. M.; Pitts, J. N., Jr. Alkyl Nitrate Formation from the Nitrogen Oxide (NO_x)-Air Photooxidations of C_2 – C_8 n-Alkanes. J. Phys. Chem. A 1982, 86, 4563–4569.
- (24) Arey, J.; Obermeyer, G.; Aschmann, S. M.; Chattopadhyay, S.; Cusick, R. D.; Atkinson, R. Dicarbonyl Products of the OH Radical-Initiated Reaction of a Series of Aromatic Hydrocarbons. *Environ. Sci. Technol.* **2009**, *43*, 683–689.
- (25) Yu, J.; Jeffries, H. E.; Le Lacheur, R. M. Identifying Airborne Carbonyl Compounds in Isoprene Atmospheric Photooxidation Products by Their PFBHA Oximes Using a Gas Chromatography/lon Trap Mass Spectrometry. *Environ. Sci. Technol.* **1995**, *29*, 1923–1932.
- (26) Matsunaga, A.; Ziemann, P. J. Gas-Wall Partitioning of Organic Compounds in a Teflon Film Chamber and Potential Effects on Reaction Product and Aerosol Yield Measurements. *Aerosol Sci. Technol.* **2010**, *44*, 881–892.
- (27) Yeh, G. K.; Ziemann, P. J. Gas-Wall Partitioning of Oxygenated Organic Compounds: Measurements, Structure–Activity Relationships, and Correlation with Gas Chromatographic Retention Factor. *Aerosol Sci. Technol.* **2015**, *49*, 727–738.
- (28) Ranney, A. P.; Ziemann, P. J. Identification and Quantification of Oxidized Organic Aerosol Compounds using Derivatization, Liquid Chromatography, and Chemical Ionization Mass Spectrometry. *Aerosol Sci. Technol.* **2017**, *51*, 342–353.
- (29) Grosjean, D.; Grosjean, E.; Williams, E. L. Atmospheric Chemistry of Unsaturated Alcohols. *Environ. Sci. Technol.* **1993**, 27, 2478–2485.
- (30) Pankow, J. F. An Absorption Model of the Gas/Aerosol Partitioning of Organic Compounds in the Atmosphere. *Atmos. Environ.* **1994**, 28, 185–188.
- (31) Pankow, J. F.; Asher, W. E. SIMPOL.1: A Simple Group Contribution Method for Predicting Vapor Pressures and Enthalpies of Vaporization of Multifunctional Organic Compounds. *Atmos. Chem. Phys.* **2008**, *8*, 2773–2796.
- (32) Nishino, N.; Arey, J.; Atkinson, R. Rate Constants for the Gas-Phase Reactions of OH Radicals with a Series of C_6 - C_{14} Alkenes at 299 \pm 2 K. J. Phys. Chem. A **2009**, 113, 852–857.
- (33) Arey, J.; Aschmann, S. M.; Kwok, E. S. C.; Atkinson, R. Alkyl Nitrate, Hydroxyalkyl Nitrate, and Hydroxycarbonyl Formation from the NO_x -Air Photooxidations of C_5 – C_8 n-Alkanes. J. Phys. Chem. A **2001**, 105, 1020–1027.
- (34) Reisen, F.; Aschmann, S. M.; Atkinson, R.; Arey, J. 1,4-Hydroxycarbonyl Products of the OH Radical-Initiated Reactions of C_5 – C_8 n-Alkanes in the Presence of NO. *Environ. Sci. Technol.* **2005**, 39, 4447–4453.
- (35) Yeh, G. K.; Ziemann, P. J. Identification and Yields of 1,4-Hydroxynitrates Formed from the Reactions of $\rm C_8-C_{16}$ *n*-Alkanes

- with OH Radicals in the Presence of NOx. J. Phys. Chem. A 2014, 118, 8797-8806.
- (36) Atkinson, R. Gas-Phase Tropospheric Chemistry of Volatile Organic Compounds: 1. Alkanes and Alkenes. *J. Phys. Chem. Ref. Data* 1997, 26, 215–290.
- (37) Atkinson, R. Rate Constants for the Atmospheric Reactions of Alkoxy Radicals: An Updated Estimation Method. *Atmos. Environ.* **2007**, *41*, 8468–8485.
- (38) Aimanant, S.; Ziemann, P. J. Development of Spectrophotometric Methods for the Analysis of Functional Groups in Oxidized Organic Aerosol. *Aerosol Sci. Technol.* **2013**, *47*, 581–591.
- (39) Millefiori, S.; Millefiori, A.; Guerrera, F. Effects of Intramolecular Hydrogen Bonding on the Absorption Transition Energies of 2-Hydroxy-5-Methylazobenzene. *Spectrochim. Acta, Part A* **1980**, 36, 835–837.
- (40) Atkinson, R.; Arey, J. Atmospheric Degradation of Volatile Organic Compounds. *Chem. Rev.* **2003**, *103*, 4605–4638.
- (41) Peng, Z.; Jimenez, J. L. KinSim: A Research-Grade, User-Friendly, Visual Kinetics Simulator for Chemical-Kinetics and Environmental-Chemistry Teaching. *J. Chem. Educ.* **2019**, *96*, 806–811.
- (42) Ziemann, P. J.; Atkinson, R. Kinetics, Products, and Mechanisms of Secondary Organic Aerosol Formation. *Chem. Soc. Rev.* **2012**, *41*, 6582–6605.
- (43) Finewax, Z.; Jimenez, J. L.; Ziemann, P. J. Development and Application of a Low-Cost Vaporizer for Rapid, Quantitative, In Situ Addition of Organic Gases and Particles to an Environmental Chamber. *Aerosol Sci. Technol.* **2020**, *54*, 1567–1578.
- (44) Vereecken, L.; Peeters, J. Decomposition of Substituted Alkoxy Radicals-Part I: A Generalized Structure-Activity Relationship for Reaction Barrier Heights. *Phys. Chem. Chem. Phys.* **2009**, *11*, 9062–9074.
- (45) Vereecken, L.; Peeters, J. A Structure-Activity Relationship for the Rate Coefficient of H-Migration in Substituted Alkoxy Radicals. *Phys. Chem. Chem. Phys.* **2010**, *12*, 12608–12620.
- (46) O'Brien, J. M.; Czuba, E.; Hastie, D. R.; Francisco, J. S.; Shepson, P. B. Determination of the Hydroxy Nitrate Yields from the Reaction of C_2 – C_6 Alkenes with OH in the Presence of NO. *J. Phys. Chem. A* **1998**, *102*, 8903–8908.
- (47) Zhang, J.; Dransfield, T.; Donahue, N. M. On the Mechanism for Nitrate Formation via the Peroxy Radical + NO Reaction. *J. Phys. Chem. A* **2004**, *108*, 9082–9095.

Supporting Information

Comprehensive Analysis of Products and the Development of a Quantitative Mechanism for the OH Radical-Initiated Oxidation of 1-Alkenes in the Presence of NO_x

Julia G. Bakker-Arkema^{†,‡}, Paul J. Ziemann^{†,‡,*}

- † Cooperative Institute for Research in Environmental Sciences (CIRES), Boulder, Colorado 80309, United States
- ‡ Department of Chemistry, University of Colorado, Boulder, Colorado 80309, United States

Abstract. Mechanisms of H atom abstraction without (Scheme S1) and with (Scheme S3) values of branching ratios and for OH radical addition (Scheme S2) with values of branching ratios for reactions of 1-alkenes with OH radicals in the presence of NO_x; complex gradient elution method from Karst et al.¹ (Figure S1); HPLC calibration curves for 2-ethylhexyl nitrate and authentic dihydroxynitrate and 1,4-hydroxynitrate standards (Figure S2); HPLC chromatogram for derivatized 6-hydroxy-5-decanone and the corresponding absorbance ratio (430 nm/360 nm) (Figure S3) and the CI-ITMS mass spectra of the 6-hydroxy-5-decanone hydrazones (Figure S4); and reactions and rate constants used in the KinSim kinetic model (Table S1).

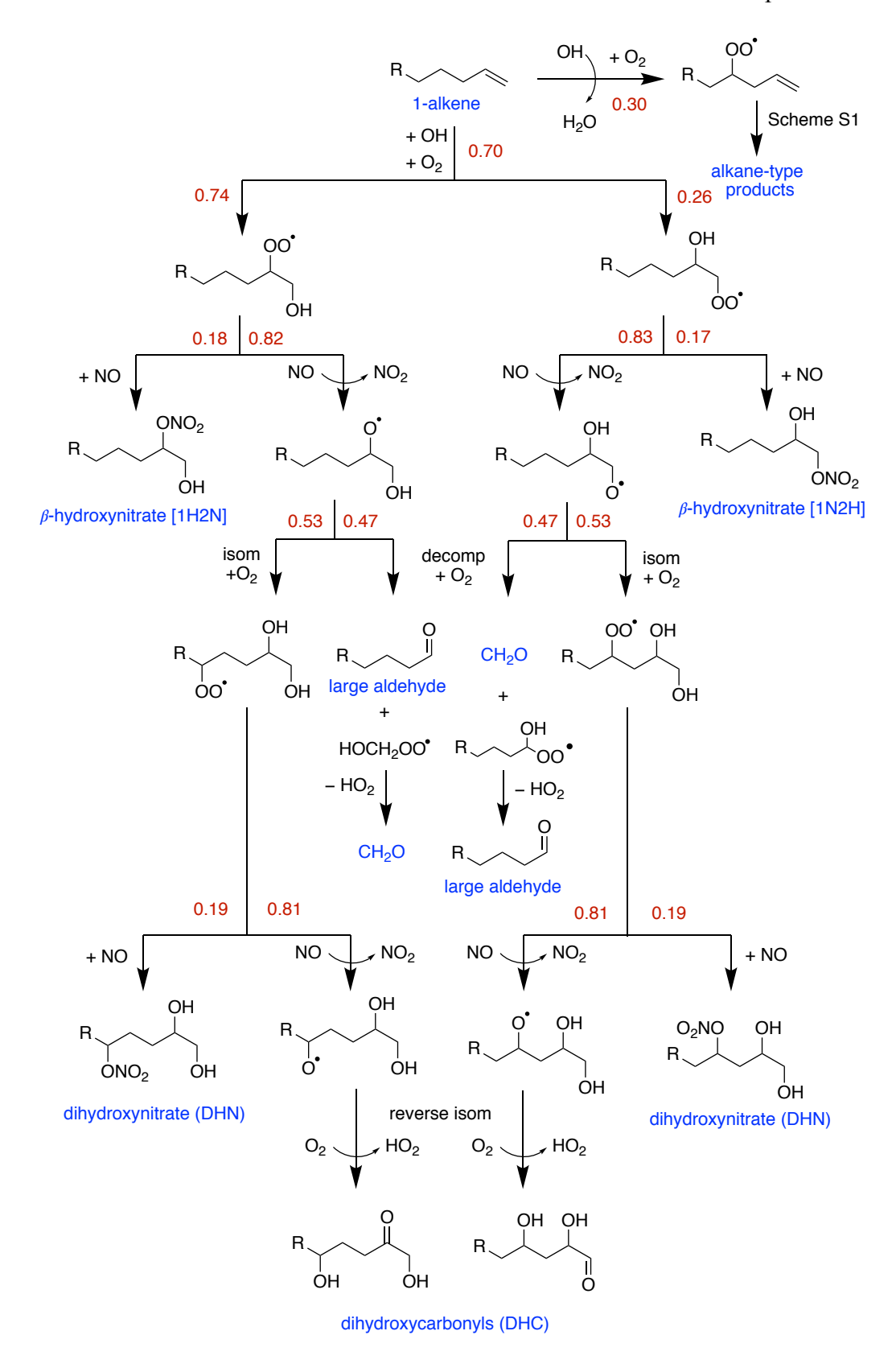
References

(1) Karst, U.; Binding, N.; Cammann, K.; Witting, U. Interferences of Nitrogen Dioxide in the Determination of Aldehydes and Ketones by Sampling on 2,4-Dinitrophenylhydrazine-Coated Solid Sorbent. *Fresenius J. Anal. Chem.* **1993**, *345*, 48–52.

Scheme S1. Mechanism for the H atom abstraction pathway in the reaction of 1-alkenes with OH radicals in the presence of NO_x .

1,4-hydroxycarbonyl [1,4-HC]

Scheme S2. Mechanism for the reaction of 1-alkenes with OH radicals in the presence of NO_x.



Scheme S3. Mechanism for the H atom abstraction pathway in the reaction of 1-alkenes with OH radicals in the presence of NO_x .

1,4-hydroxycarbonyl [1,4-HC]

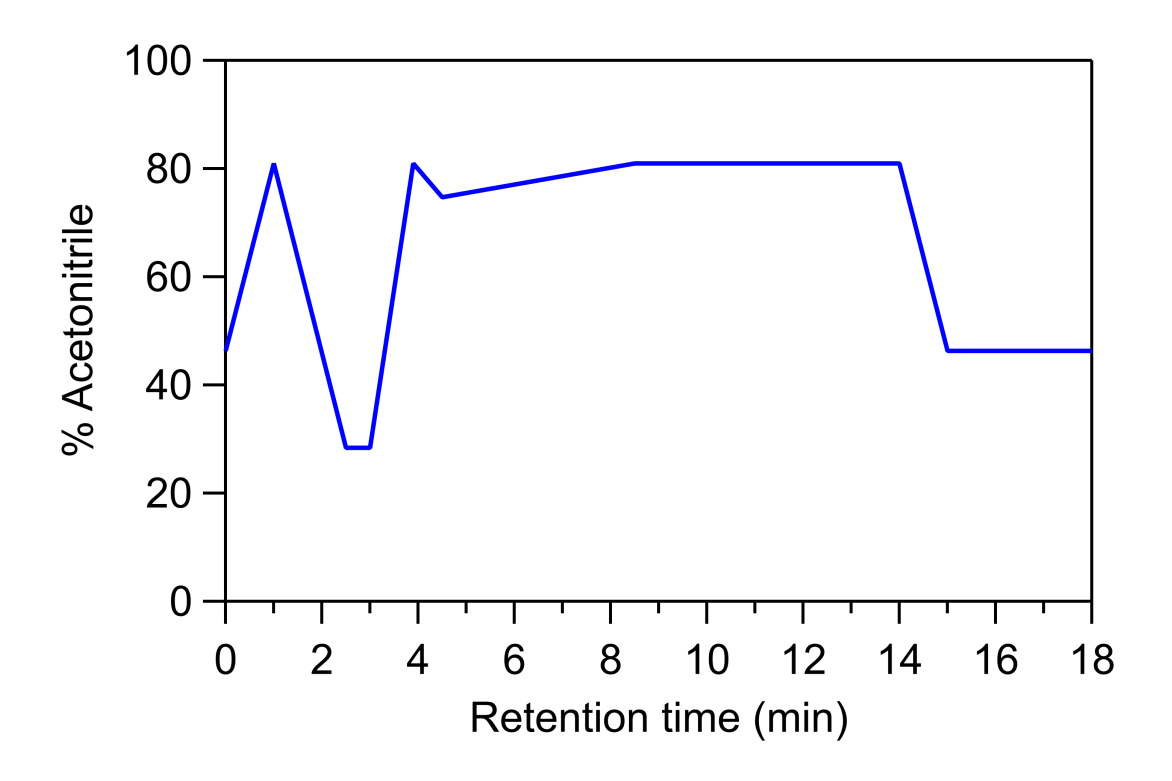


Figure S1. Complex gradient elution method adapted from Karst et al. (1993).

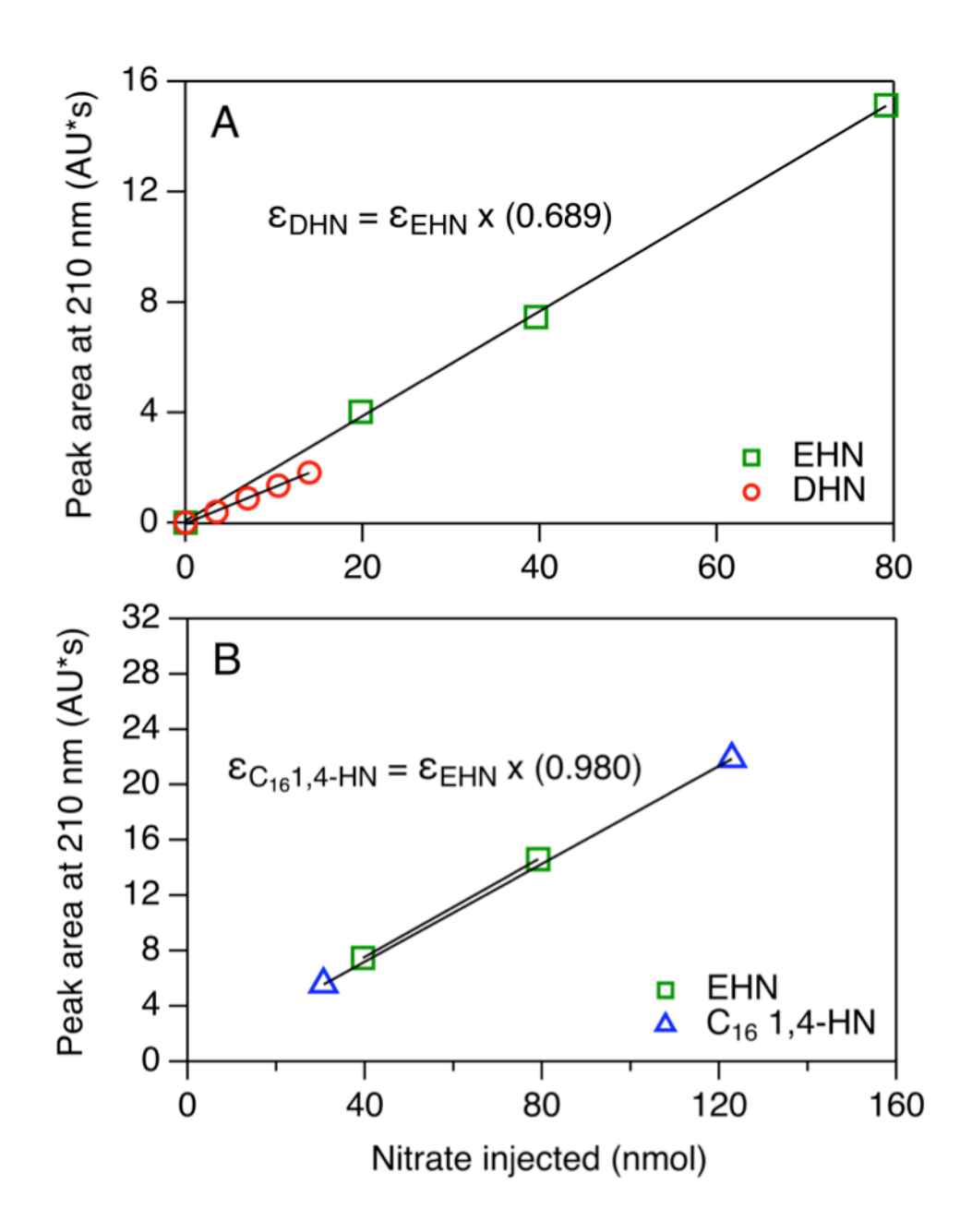


Figure S2. (A) Calibration curves for an authentic dihydroxynitrate (DHN) standard and a 2-ethylhexyl nitrate (EHN) standard that was to quantify 1,4-hydroxynitrates, where the uncertainties in the slopes for DHN and EHN are 2.0% and 1.6%, respectively. (B) Calibration curves for a purified mixture of C_{16} 1,4-hydroxynitrate isomers (C16 1,4-HN) formed from the reaction of *n*-hexadecane with OH radicals in the presence of NO_x and for EHN, both measured during a different study.

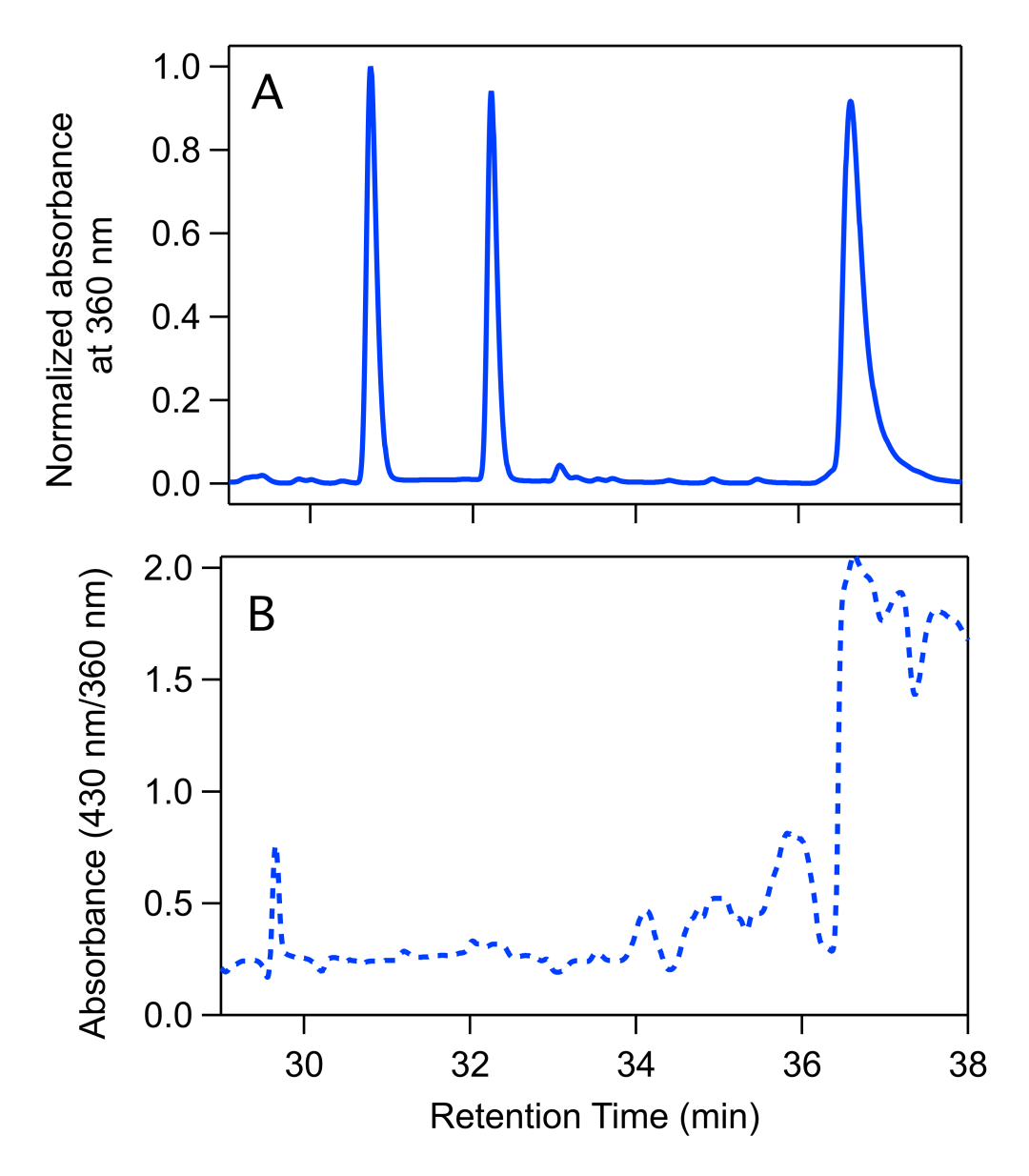


Figure S3. HPLC chromatogram monitored at 360 nm (A) for derivatized 6-hydroxy-5-decanone, a surrogate standard for quantifying dihydroxycarbonyl reaction products; and (B) the ratio of the 430 nm/360 nm absorbance for the same chromatogram.

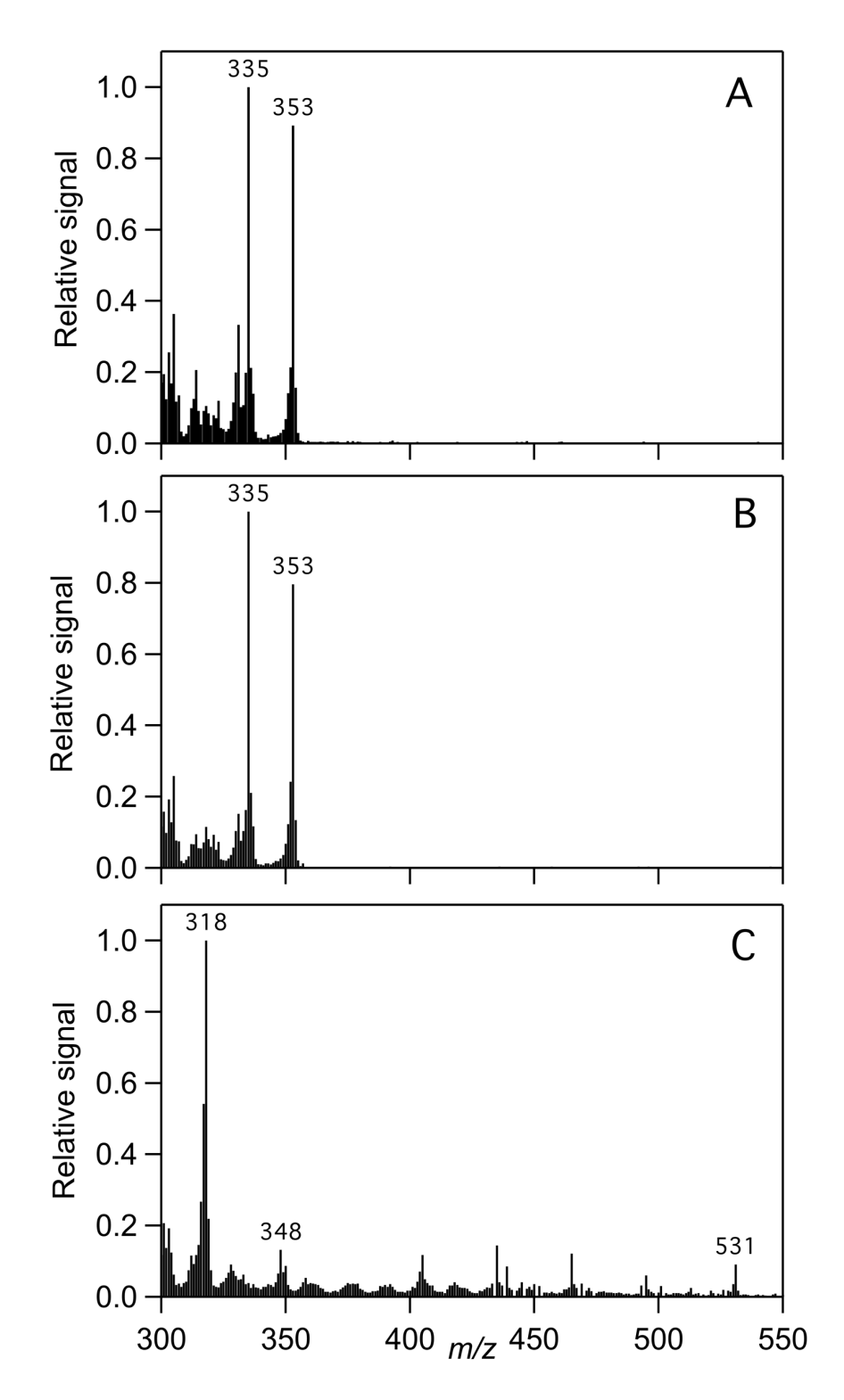


Figure S4. CI-ITMS mass spectra for the fractionated peaks of derivatized 6-hydroxy-5-decanone for peak 1 (A), peak 2 (B), and peak 3 (C). 353 = [M+1] and $335 = [M+1] - H_2O$ for the singly derivatized hydrazone. $531 = [M+1] - H_2$ for the doubly derivatized hydrazone.

Table S1. Reactions and rate constants used in the KinSim model to correct measured C_{13} and C_{14} aldehyde yields for gas-wall partitioning and secondary reactions with OH radicals.

Reaction	Rate constant	
1-tetradecene + OH → tridecanal + other products	$5.2 \times 10^{-11} \text{ cm}^3 \text{ molec}^{-1} \text{ s}^{-1}$	
tridecanal + OH → secondary reaction products	$3.7 \times 10^{-11} \text{cm}^3 \text{molec}^{-1} \text{s}^{-1}$	
tridecanal (gas) → tridecanal (wall)	$8.7 \times 10^{-4} \text{ s}^{-1}$	
tridecanal (wall) → tridecanal (gas)	$4.1 \times 10^{-4} \text{ s}^{-1}$	
1-pentadecene + OH \rightarrow tetradecanal + other products	$5.3 \times 10^{-11} \text{ cm}^3 \text{ molec}^{-1} \text{ s}^{-1}$	
tetradecanal + OH → secondary reaction products	$3.9 \times 10^{-11} \text{ cm}^3 \text{ molec}^{-1} \text{ s}^{-1}$	
$tetradecanal (gas) \rightarrow tetradecanal (wall)$	$9.2 \times 10^{-4} \text{ s}^{-1}$	
$tetradecanal (wall) \rightarrow tetradecanal (gas)$	$3.6 \times 10^{-4} \text{ s}^{-1}$	